AIAA-91-0057

Optimization of Aerobrake Assisted Descent Trajectories at Mars

M. Cupples, J. Nordwall, S. LeDoux
T. Ruff, and G. Woodcock
Boeing Aerospace and Electronics
Huntsville, AL

29th Aerospace Sciences Meeting
January 7–10, 1991/Reno, Nevada

OPTIMIZATION OF AEROBRAKE ASSISTED DESCENT TRAJECTORIES AT MARS

Michael Cupples, Jill Nordwall, Stephen LeDoux, Theron Ruff,
and Gordon Woodcock
Boeing Aerospace and Electronics, Huntsville Division

Abstract

This paper examines considerations pertinent to the use and design of Martian aerobraking descent vehicles having lifting characteristics. It focuses on optimizing decent trajectories to maximize the crossrange of an aerobrake vehicle which has a maximum lift-to-drag ratio (L/D) of 1.2 and ballistic coefficient of 28 lb/ft^2. Crossrange translates into the capability of the vehicle to reach desired landing sites from a variety of minimum energy interplanetary transfers and the resulting Mars' parking orbits. This type of aerobrake was found to yield substantial crossrange of over 1000 nmi. A Mars descent aerodynamic heating analysis is also presented for the "worst case" trajectory studied, showing the maximum descent heating rate to be 8.0 BTU/ft^2 sec with a maximum temperature of 1650°F.

Introduction

Previous expeditions to the planet Mars have ranged from the fly-by of Mariner 4 (1965) to the surface landings of Vikings 1 and 2 (1976). One major consideration of current Mars mission analyses is the selection of manned landing sites. This selection is dependent on many factors that are related to mission vehicle capability and configuration, including the overall delta velocity budget of Earth departure, mid-course interplanetary corrections, method of Mars orbit capture (all propulsive or aerocapture), parking orbit size and orientation with respect to Mars, descent to surface trajectory, and return-to-Earth energy requirements. Of particular interest are the characteristics necessary to define a Mars descent to surface vehicle.

This paper examines optimized aerobrake-assisted trajectories for a descent vehicle with maximum lift-to-drag ratio (L/D)≈1.2 and described in this paper as having "medium" L/D[1]. The goal of the optimization was to maximize crossrange during a lifting descent and thereby gain an initial understanding of the landing site accessibility of this vehicle. Crossrange is defined as the lateral distance traversed by the vehicle with respect to its parking orbit ground track (Fig.1).

The vehicle descent to the Martian surface will consist of two phases: a pre-atmosphere descent phase and an atmospheric flight phase. The analysis of this paper begins at the Martian descent entry interface altitude of about 54 nmi. The minimum energy descent orbit plane is by definition coincident with the Mars parking orbit plane, established at Mars vehicle capture. In fact, the descent orbit is treated as a minor perturbation of the parking orbit (via a small delta V applied at the apoapsis). The atmospheric portion of the descent is a function of the vehicle's crossrange capability (in terms of configuration, L/D, maneuverability, and delta V constraints). Trajectory simulations presented here were performed using an implicit integration code known as Optimal Trajectories by Implicit Simulation (OTIS)[2]. OTIS uses a nonlinear programming technique for optimization and was developed by Boeing under contract to the United States Air Force. The descent trajectories were optimized by OTIS to maximize crossrange based on a fairly broad range of atmospheric and dynamic entry conditions. Control parameters varied in the simulations were roll angle and angle-of-attack.

The combination of the parking orbit established prior to descent and the vehicle's crossrange capability has a major impact on Mars landing site selection. Previous studies[3] have shown that a wide variety of landing sites may be accessed, based on crossrange, by a vehicle with maximum L/D of 2.3. A broad range of viable landing sites is also possible with a medium L/D aerobrake. This reduction in L/D results in less vehicle control mechanism complexity and a lower vehicle mass[1].

An analysis pertaining to the aerothermal environments encountered by the descent vehicle is also presented in this paper.

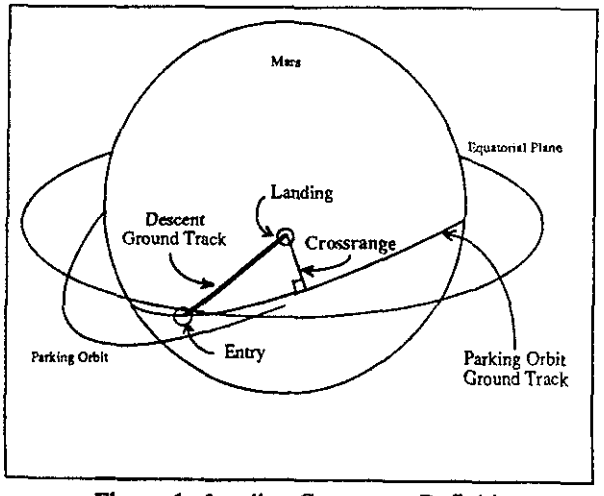

Figure 1. Landing Crossrange Definition

	Example	Operation	Geometry
	OTV studies	Drag only	Deformable
	Viking Galileo Mercury	Drag only	Axisymmetric dish
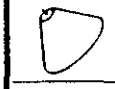	Apollo	Low L/D $\alpha \neq 0$	Axisymmetric cone/shallow dish
	OTV studies MM Mars studies	Low L/D $\alpha \neq 0$	Shallow axisymmetric dish
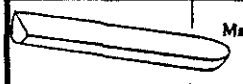	Martin FY89	Low L/D	Shaped sled
	Boeing lunar,Mars, assembly studies	Moderate L/D	Deep non-symmetric dish
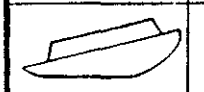	AFB	Moderate L/D	Non-symmetric raked cone
	Langley studies	Moderate L/D	Deep dish
	HL-10 M2-F2	Moderate L/D	Blunt lifting body
	MM studies, MRSR	Medium L/D $\alpha \neq 0$	Axisymmetric conic
	MRSR, Eagle studies	Medium L/D	Non-symmetric conic
	Boeing Wing	Medium L/D	Non-symmetric shallow shell
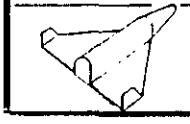	X-24 Dyna Soar, Shuttle	High L/D	Winged flyer

Figure 2. Aerobrake and Re-entry Vehicles

Discussion of Models

Descent Vehicle L/D

Vehicle L/D choice must be based on the entire mission profile for multiple year Mars opportunities, and hence L/D requirements must be tailored for several mission scenarios. Three mission flexibility related reasons for choosing a medium L/D vehicle (Fig. 2) are indicated below:

First, a lifting vehicle must provide sufficient crossrange to reach a Mars base site for missions ranging over most of the dates of current interest (opportunity years 2010 through 2025) and for landing sites of varying scientific and technical interest. For these opportunities, the Mars parking orbits corresponding to each minimum energy interplanetary trajectory fall within planes that tend to vary widely in terms of inclination and periapsis latitude (periapsis latitude is the areographic latitude of a point found by projecting the periapsis onto the surface of Mars in the nadir direction from periapsis). As a result, parking orbits established by any two opportunities may, in general, vary greatly. Thus, a base established by a previous mission may not be accessible to succeeding missions unless the lander is capable of adequate crossrange; sufficient crossrange can be obtained from a medium L/D vehicle to reach many Mars sites of interest[4] (Fig. 3). In addition, a maneuverable lifting descent

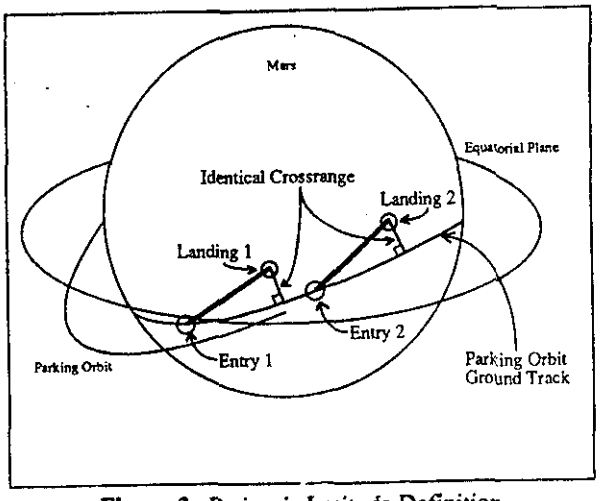

Figure 3. Periapsis Latitude Definition

vehicle is seen as a viable and more efficient solution to this crossrange problem than a mid-course targeting maneuver intended to establish a parking orbit with periapsis near the landing site latitude and with the required inclination. The propellant required for such a manuever would be prohibitively expensive[5].

A second issue is astronaut safety, relating to Mars parking orbit periapsis lighting angle (periapsis lighting angle is the elevation of the sun above the horizon at the point on Mars' surface in the nadir direction from parking orbit periapsis). Essentially, missions must be designed such that the vehicle can be landed during the Martian day, providing light adequate for avoidance of hazardous terrain. A medium L/D vehicle will provide flexibility in the event that the periapsis lighting angle is small, forcing the lander to fly beyond the daylight terminator and then maneuver back to a daylight landing site (Fig. 4).

Lastly, the relationship that a medium L/D vehicle has with aerocapture must be considered. Analysis shows that for a particular range of entry velocities, there is a need for at least a medium L/D vehicle to be used for effective aerocapture[4]. This medium L/D vehicle will provide aerocapture control authority necessary to compensate for uncertainties in knowledge of the local Mars atmosphere, planetary navigation errors, and trim angle-of-attack[6]. This is a significant factor when the aerocapture vehicle also serves as the descent and landing vehicle.

Aerodynamic Vehicle Model

A mission-configured medium L/D aerobrake concept is shown in Figure 5. This aerodynamic shape was derived from a

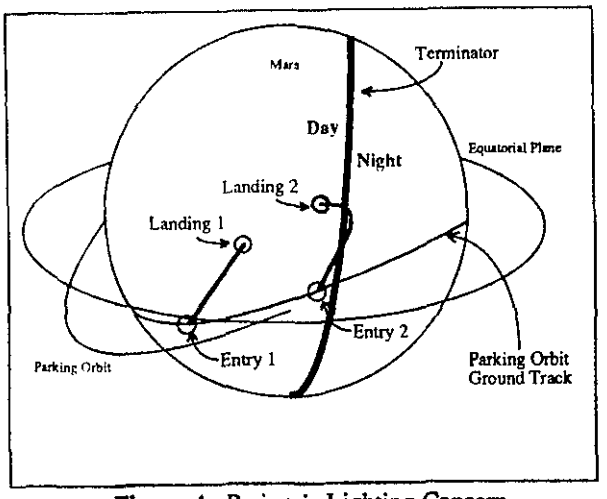

Figure 4. Periapsis Lighting Concern

family of biconics and has evolved into a flatter shape for improved packaging, module and system configuration, and landing flare maneuvering. It consists of a rotated hyperboloid (large eccentricity) cut from the top view with a truncated hyperbola, with the addition of a blunted lip along the leading edge. Some features added to the basic aerodynamic model (Fig. 6) will be needed for control and thermal protection purposes, and are shown on the fully configured vehicle displayed in Figure 5. These features include control surfaces, such as rear-body flaps and vertical stabilizers, as well as an aftbody shroud designed to protect the cargo and/or manned vehicle from high temperature flows incurred during atmospheric entry.

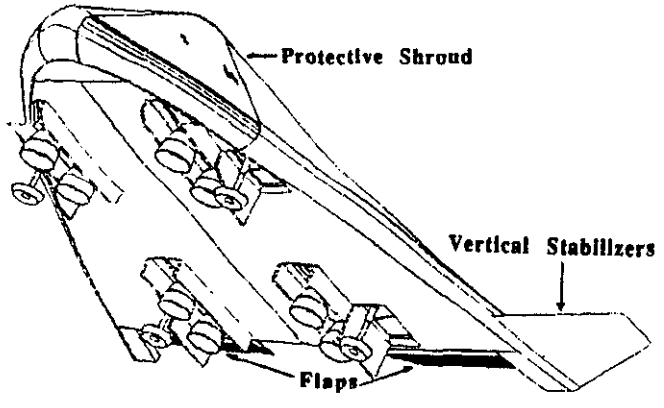

Figure 5. Fully Configured Medium L/D Descent Vehicle

Preliminary analyses were performed using the body shown in Figure 6. Hypersonic aerodynamic predictions for this shape were based on modified Newtonian Impact Theory[7,8], with the lift and drag forces computed by integrating the theoretical pressures over the lifting surface of the vehicle, and resolving the net force in the lift and drag directions. The predicted values of coefficient of lift (C_L), coefficient of drag (C_D), and L/D used in this study are shown in Figure 7 as a function of angle-of-attack (AOA). The axes used for defining the roll angle, AOA, and flight path angle (FPA) are illustrated in

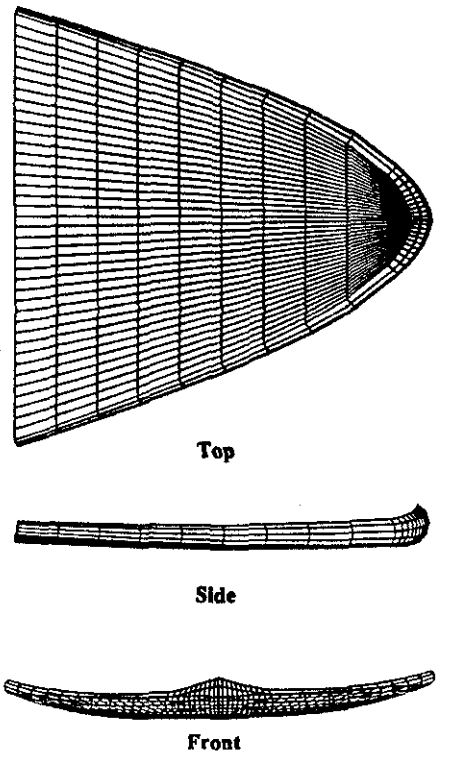

Figure 6. Aerodynamic Vehicle Model

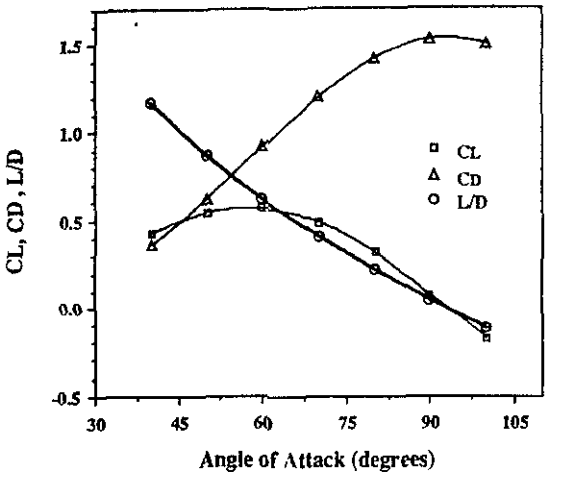

Figure 7. Aerodynamic Properties

Figure 8. Resultant force vectors for this shape are displayed in Figure 8, where the trim AOA is 40° for an L/D of 1.2.

From a packaging standpoint, the resultant force distribution is favorable, in that the center of gravity of the fully configured vehicle can be located far aft of the leading edge for proper trim. Considering the stability and control aspects, this distribution shows that only small pitching moments are needed to perturb the vehicle (the angular spread of the resultant force lines indicates the stability characteristics: the wider the spread, the more stable the vehicle). Thus the need for flaps, as shown in Figure 5, to keep the vehicle properly trimmed. For AOA

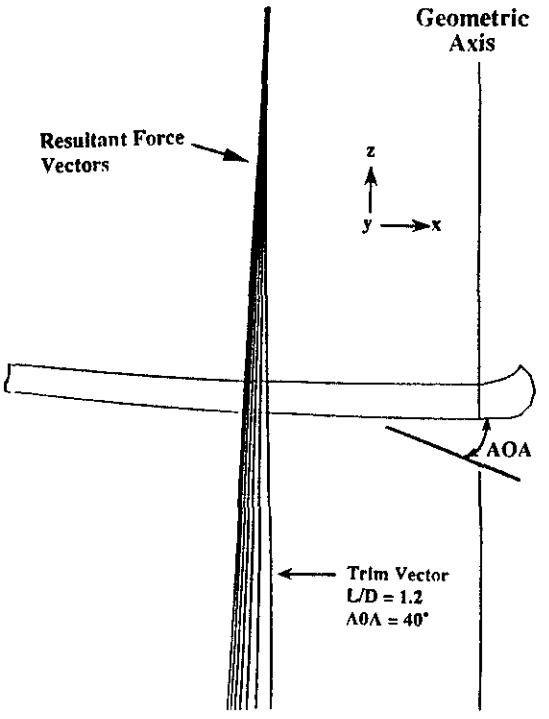

Figure 8. Resultant Force Distribution

control (used in some of the descent trajectories presented herein), this resultant force spread is advantageous as small moments, such as the deflection of flaps, suffice in pitching the vehicle up or down. In contrast, the blunt low L/D vehicles (Figure 2) are very stable (see Figure 9 for an example) and require large pitching moments for AOA variation. Since these

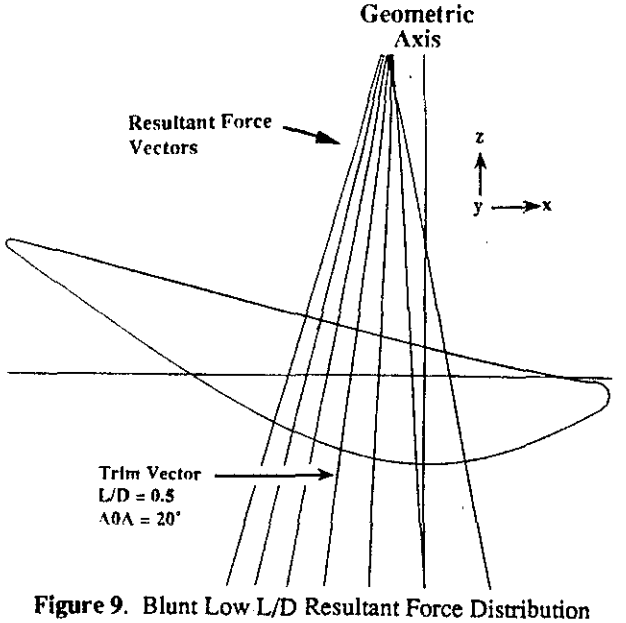

Figure 9. Blunt Low L/D Resultant Force Distribution

low L/D vehicles use reaction control jets for AOA variation, this proves to be very costly in terms of propellant mass, which is one of the main reasons the flatter medium L/D vehicle was derived. The blunt low L/D vehicles are also practically incapable of performing a flare maneuver (desired in the terminal part of the descent), which can easily be performed with the medium L/D vehicle (using flap control).

Mars Atmosphere Model

In this section, a definition is given of the Mars atmosphere models upon which the simulations presented in this paper were based. The optimized descent trajectories presented herein used high, average, and low Mars equatorial atmosphere density profiles. These profiles, as shown in Figure 10, were generated by the Mars Global Reference Atmosphere Model (MarsGRAM)[9] for the year 2016. The extremes and the average represent measurements taken at the two solstices and spring equinox, respectively.

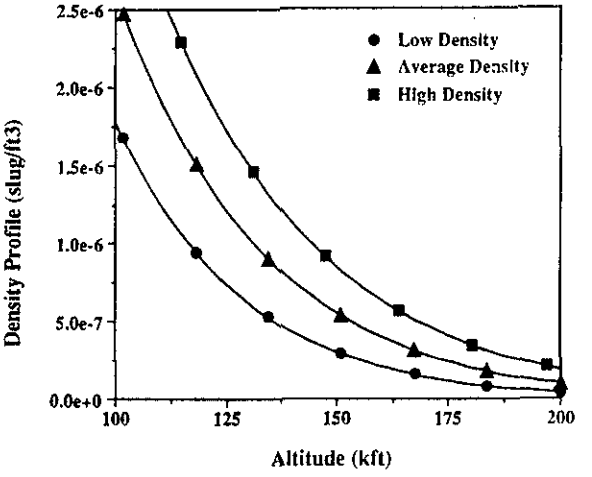

Figure 10. MarsGRAM Density vs Altitude of Interest

Discussion of Descent Trajectories

To initiate the descent trajectory, a minimum energy maneuver is performed at the apoapsis of the parking orbit. Essentially, this descent maneuver consists of a lowering of periapsis to an altitude of approximately 25 nmi. The vehicle then descends from apoapsis to encounter the Martian atmosphere at entry interface. For a one solar day parking orbit, the descent maneuver translates to an entry interface velocity of 14.8 kft/sec at an altitude of 322 kft .

Upon reaching entry interface, maneuverability of the descent vehicle was examined in terms of roll angle and AOA. Two maneuvering descent scenarios were studied to understand their effect on maximized crossrange: 1) AOA (thus L/D) was held constant throughout the descent while roll angle was allowed to vary optimally; 2) Both AOA (L/D) and roll angle were allowed to vary optimally. For the first descent scenario, descent trajectory optimizations to maximize crossrange were achieved for a range of inclinations, apoapsis altitudes, and L/D values. For the second descent scenario, one particular case of inclination, apoapsis altitude, and L/D value was analyzed.

Each of the OTIS simulations were terminated with the vehicle's descent constrained to end at an altitude of 50 kft and a velocity of 1000 ft/sec. These end conditions were chosen due to possible aerobrake maneuvers occurring at this point in the descent (e.g., flare maneuvers, aeroshell jettisoning, etc.).

General Descent Discussion

A general descent trajectory profile is presented using the reference aerobrake with L/D equal to 1.0. The descent orbit is defined with an inclination of 15°, apoapsis altitude of 20,000 nmi, periapsis altitude of 25 nmi and with initial latitude and longitude of zero degrees. This general trajectory is further constrained by forcing a constant AOA (equal to 46°, providing an L/D of about 1.0). A high density Martian atmosphere (Fig. 10) was assumed for this descent simulation.

The altitude and velocity profiles, with the simulation ending at the prescribed conditions, are shown in Figures 11 and 12 respectively. Soon after the vehicle's initial atmosphere encounter, the OTIS optimized descent rolls the vehicle (refer to Figure 13) to create a near constant velocity trajectory . This may be seen on Figure 11 for the time between 100 and 1200 seconds. This initial maneuver is designed to move the velocity vector out of the initial descent plane (thus producing crossrange) and to drive the Flight Path Angle (FPA) to zero degrees (see Figure 14). Roll maneuvers are designed thereafter to maintain the FPA as near zero as optimally possible. Maintaining the average FPA about zero forces the average velocity vector to stay approximately within the local horizontal plane[10]. Hence, the vehicle establishes a glide-like descent to yield a maximum crossrange.

Referring again to Figure 13, the vehicle is seen to perform significant roll maneuvers near the end of descent. At this point, the simulation manipulates the vehicle to best satisfy three main goals: 1) The analysis is constrained to end with the vehicle reaching 50 kft at 1000 ft/sec; 2) Angle-of-attack must remain constant (no lift or drag coefficient changes); and, 3) The first two conditions must be met in the overall context of maximizing crossrange. Thus, these maneuvers are related to the optimal use of remaining vehicle energy. As may be seen in Figure 15, the crossrange steadily increases throughout the descent (these same data in terms of latitude and longitude are presented in Figure 16). This descent takes a little more than 30 minutes to traverse 855 nmi and is typical of most of the results presented in this paper.

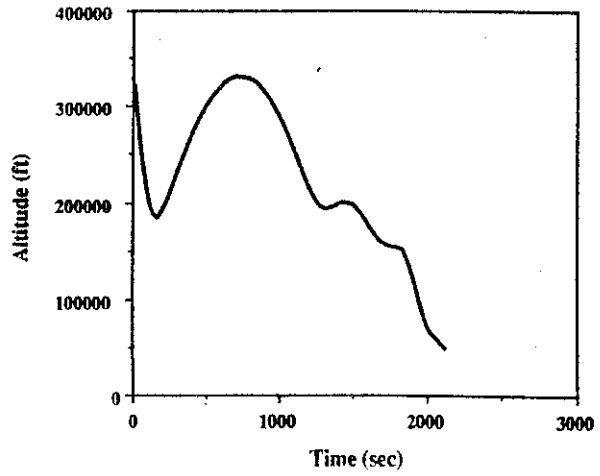

Figure 11. Altitude vs Time for General Trajectory

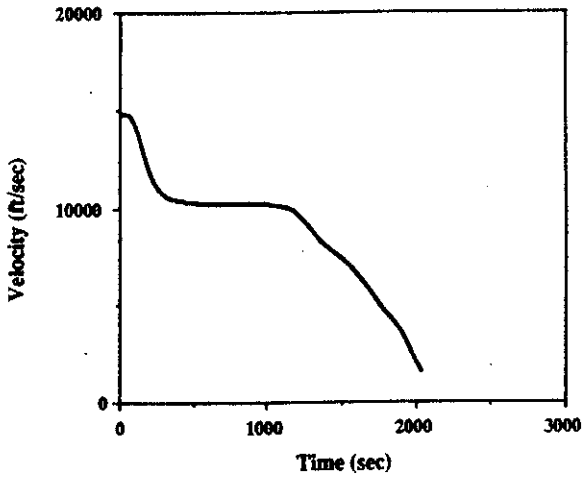

Figure 12. Relative Velocity vs Time for General Trajectory

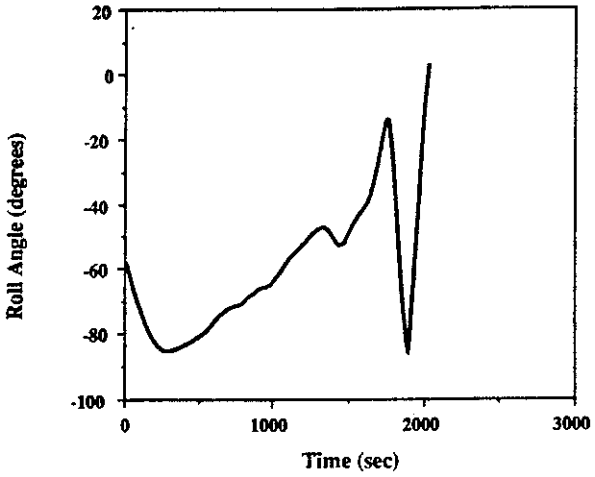

Figure 13. Roll Angle vs Time for General Trajectory

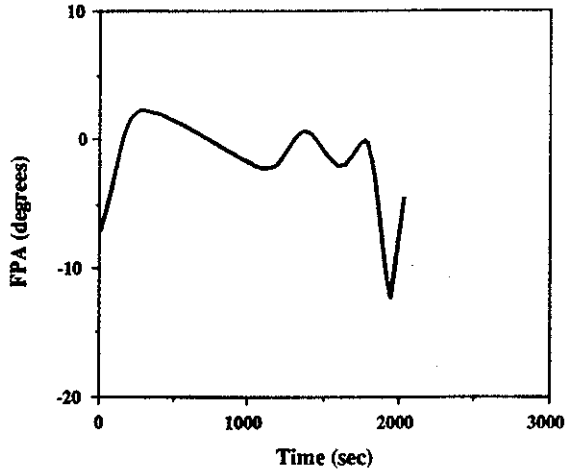

Figure 14. Flight Path Angle vs Time for General Trajectory

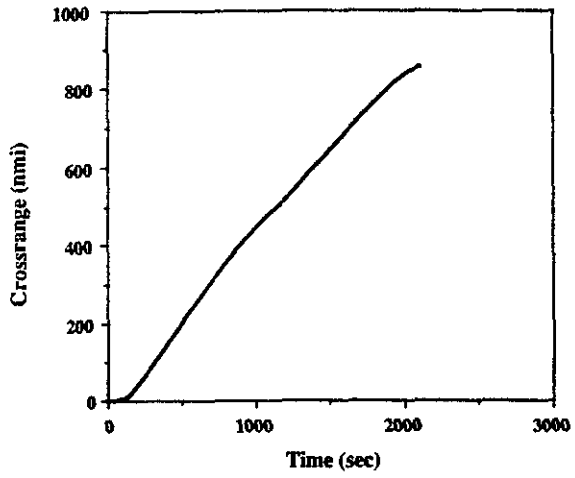

Figure 15. Crossrange vs Time for General Trajectory

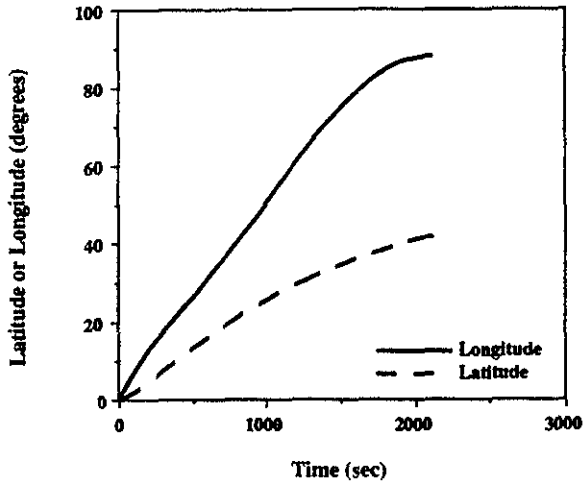

Figure 16. Latitude/Longitude vs Time for General Trajectory

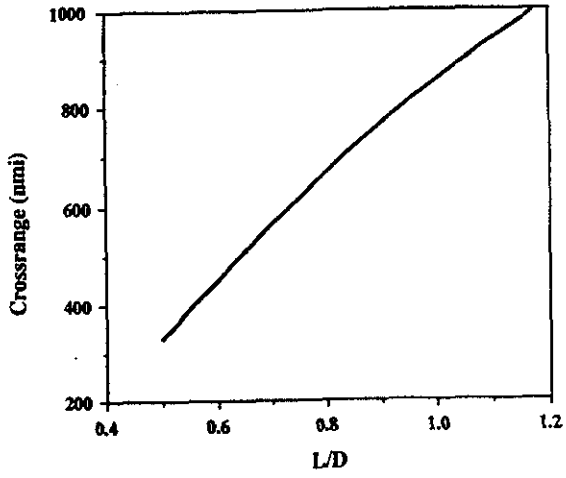

Figure 17. Crossrange vs L/D for Apo=20000 nmi, Per=25 nmi, i=15°

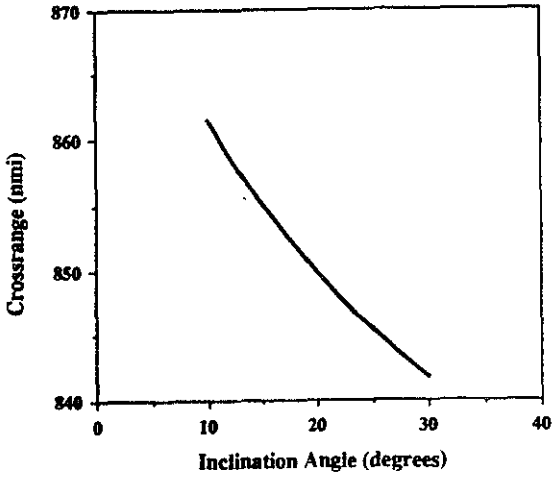

Figure 18. Crossrange vs Inclination Angle for Apo=20000 nmi, Per=25 nmi, L/D=1.0

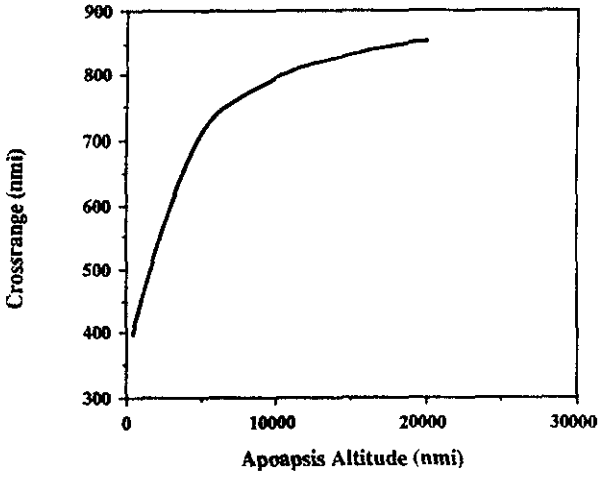

Figure 19. Crossrange vs Apoapsis Altitude for Per=25 nmi, i=15°, L/D=1.0

Parametric Discussion

A parametric study was performed to show the effect on crossrange of varying L/D as well as the following descent orbit parameters: inclination, apoapsis altitude, and the Martian atmosphere density from MarsGRAM. As Figure 17 illustrates, crossrange increases almost linearly with L/D, ranging from a value of just over 300 nmi for an L/D of 0.5 to nearly 1000 nmi for an L/D of 1.2. Similarly, crossrange decreases almost linearly, but very slightly, with increasing inclination angle (Fig. 18). Thus, crossrange is nearly independent of initial inclination.

Increasing apoapsis altitude (which is equivalent to increasing orbital energy) tends to increase crossrange; this effect, as shown in Figure 19, begins to level off above an apoapsis altitude of 10,000 nmi. This leveling off of crossrange is due in part to the entry velocity varying as shown:

$$\sqrt{(V^2_{esc} - \mu/\text{semi-major axis})},$$

where Vesc is the escape velocity at entry interface altitude and μ is the Mars gravitational parameter. Thus, given that the periapsis altitude remains constant, entry velocity approaches escape velocity asymptotically as the apoapsis altitude increases. These same data in terms of final latitude and longitude versus descent orbit inclination and apoapsis altitude are shown in Figures 20 and 21.

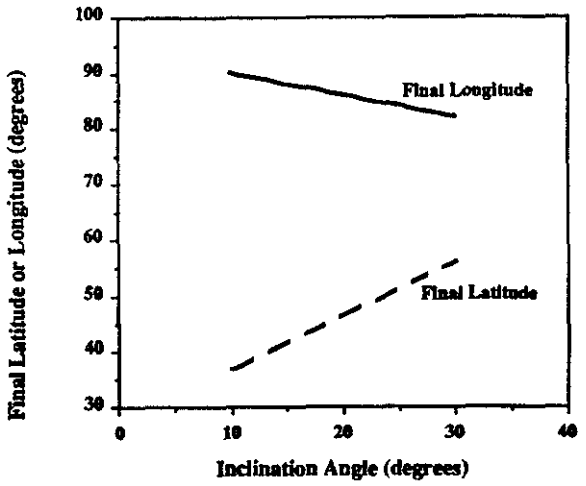

Figure 20. Final Latitude/Longitude vs Inclination Angle for Apo=20000 nmi, Per=25 nmi, L/D=1.0

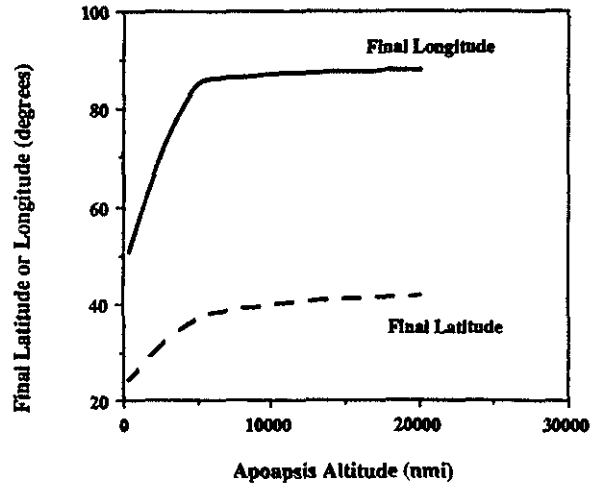

Figure 21. Final Latitude/Longitude vs Apoapsis Altitude for Per=25 nmi, i=15°, L/D=1.0

Achievable crossrange for certain MarsGRAM atmospheres (high, average, and low densities) is compared in Figure 22 (these data are representative, but not fully optimized, solutions). As shown, density changes have an almost negligible effect on crossrange (which increases only 3% from a low to a high density atmosphere). These results are due to the fact that L/D is held constant and is identical for each of the three density cases; crossrange has been shown to be dependent upon L/D. Therefore, the vehicle is able to fly a longer duration gliding descent for higher density atmospheres but does not appreciably increase its total crossrange.

Angle-of-attack Variations

As discussed above, optimized trajectories were analyzed in which roll angle was allowed to vary, but AOA was held constant (Figures 11 through 22). This section presents a study of roll angle and crossrange made for varying AOA (Figures 23 and 24); in all cases, roll angle was allowed to vary optimally. Note that allowing angle-of-attack to change tends to smooth out the descent roll maneuvers (Fig. 23). Moreover, the achieved crossrange is also improved if AOA is not constrained (Fig. 24). This increase in crossrange (over the maximum L/D, constant AOA case) may be due to a more efficient use of the vehicle's energy throughout the descent by varying the AOA (Fig. 25) instead of exclusively rolling the vehicle. As shown in these figures, AOA is held fairly constant until the last 5 minutes of the descent, at which time the vehicle pitches slightly forward and then back to increase the AOA by more than 15°. This AOA maneuver is seen to satisfy the same goals as the general trajectory's end roll maneuvers, but to do so in a less chaotic manner.

Aerothermodynamic Heating

A major factor in descent vehicle design is aerodynamic heating. Descent heating has therefore been examined to determine the thermal environments imposed on the medium L/D descent vehicle along the maximized crossrange trajectories simulated here. Heating evaluations were made at the stagnation point, at a point on the leading edge where the sweep angle is

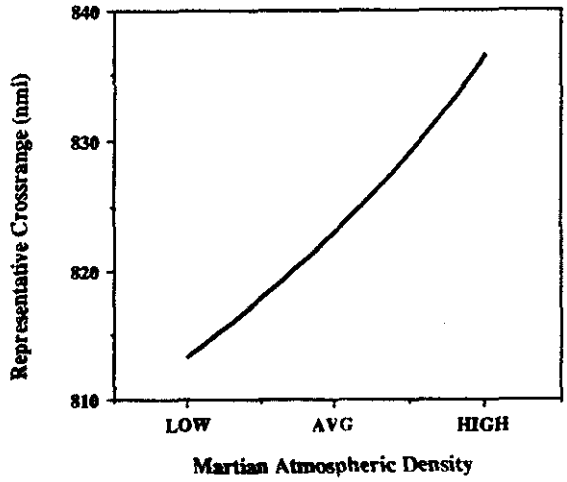

Figure 22. Representative Crossrange vs Martian Atmospheric Density for Apo=20000 nmi, Per=25 nmi, i=15°, L/D=1.0

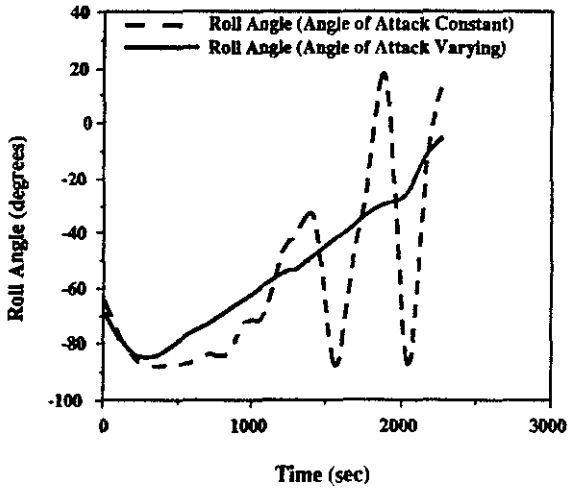

Figure 23. Roll Angle vs Time Comparison of Constant (L/D=1.17) and Varying Angle-of-attack for Apo=20000 nmi, Per=25 nmi, i=15°

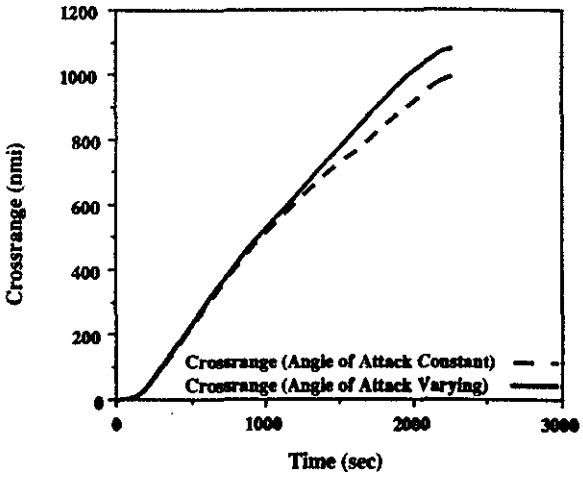

Figure 24. Crossrange vs Time Comparison of Constant (L/D=1.17) and Varying Angle-of-attack for Apo=20000 nmi, Per=25 nmi, i=15°

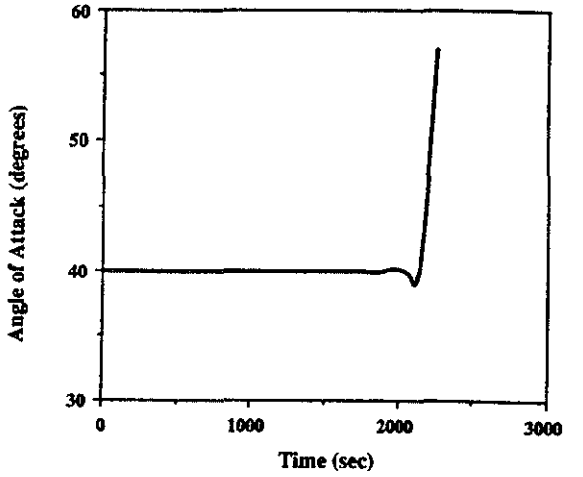

Figure 25. Varying Angle-of-attack vs Time for Apo=20000 nmi, Per=25 nmi, i=15°

70°, and along the forebody centerline for the medium L/D vehicle. Convective stagnation point and leading edge heating predictions along these trajectories were calculated using stagnation point theory and swept cylinder theory respectively[11,12]. The distributed centerline heating rates and temperatures were predicted using the Boeing Boundary Layer Analysis Program (BLAP) with thermodynamic and transport properties related to a CO_2 atmosphere[13]. Although, in Mars' predominantly CO_2 atmosphere, radiative heating will be negligible for velocities below approximately 19.7 kft/sec (for every case studied, Mars descent velocities remained below 16.4 kft/sec), calculations were made to examine the extent of radiative heating at the most severe part of the trajectory[14]. Radiative predictions were based on the results presented in reference 15. Total heating loads and peak equilibrium wall temperatures were investigated also.

An examination of maximum dynamic pressure was used as an indicator for maximum stagnation point heating for all descent trajectories; that is, the maximum dynamic pressure tends to occur at or near the same conditions as maximum stagnation point heating. The largest dynamic pressures were encountered for the high density atmosphere with varying AOA trajectory (using the general entry conditions) as shown in Figure 26.

For this "worst case" trajectory, the maximum heating occurred at 120 seconds (bottom of initial atmosphere encounter, shown in Figure 27), at an altitude of 183 kft, and a velocity of 13.9 kft/sec. At the stagnation point and along the leading edge the convective heating rate was 8 BTU/ft^{2}sec and 2.7 BTU/ft^{2}sec respectively. At this maximum convective heating point a calculation was made to determine the magnitude of the radiative heating. Using the tables in reference 15, the approximate maximum radiative heating was 2.4 x 10^{-5} BTU/ft^{2}sec. Due to this negligible value, radiative heating was not considered along the rest of the trajectory. The convective heating rates for the entire trajectory are presented in Figure 27. Shown in Figure 28 are the stagnation point and leading edge integrated heating loads for the descent trajectory. The stagnation point nose radius is 6.46 ft, and from the stagnation point the leading edge radius (or lip) is tapered from 6.47 ft to 1.97 ft at the rear of the vehicle. This reduction in nose radius is justified since the sweep angle is varied from ~45° to 70° (a function of the hyperbola shape), resulting in decreasing normal velocities and thus reduced heating. The low heating rates presented are also a result of the small ballistic coefficient of 28 lb/ft^2. Equilibrium wall temperatures were also calculated along this "worst case" trajectory and are shown in Figure 29.

The centerline convective heating for the medium L/D vehicle was examined at the maximum stagnation point heating conditions at 120 seconds. These centerline heating rates are presented in Figure 30, and the corresponding equilibrium wall temperatures, with an assumed wall emissivity of 0.8, are shown in Figure 31. The resulting temperature distribution for the medium L/D vehicle is given in Figure 32. With these relatively low wall temperatures (maximum of 1650°F), some form of hot structure thermal protection system would be adequate for this vehicle.

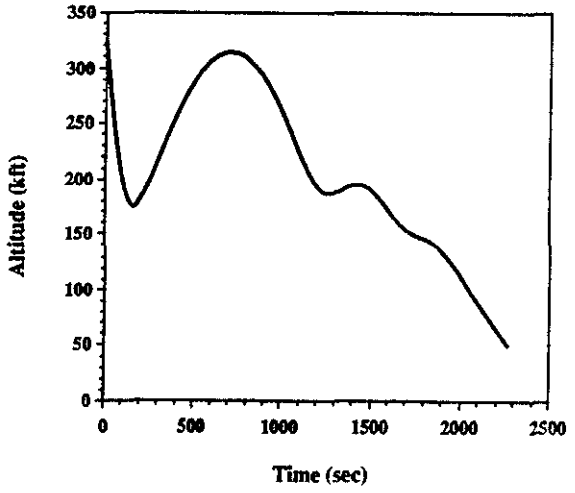

Figure 26. "Worst Case" Trajectory Using High Density Atmosphere, Varying AOA, and General Trajectory Parameters

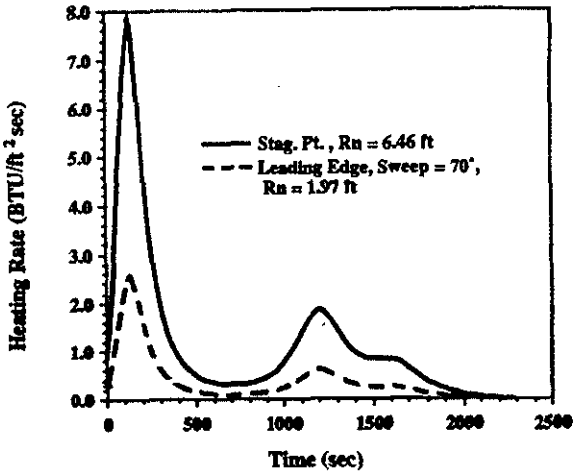

Figure 27. Convective Heating Along "Worst Case" Trajectory

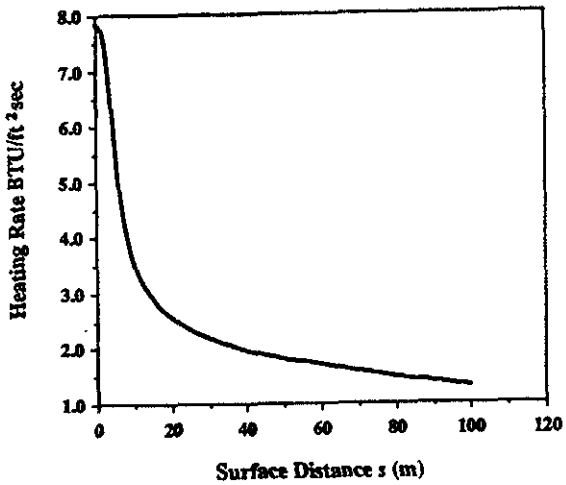

Figure 30. Convective Heating Rates Along Centerline (laminar)

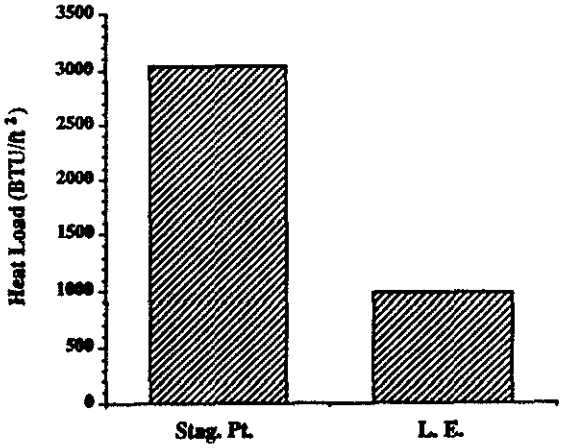

Figure 28. Integrated Heat Load at the Stagnation Point and Leading Edge

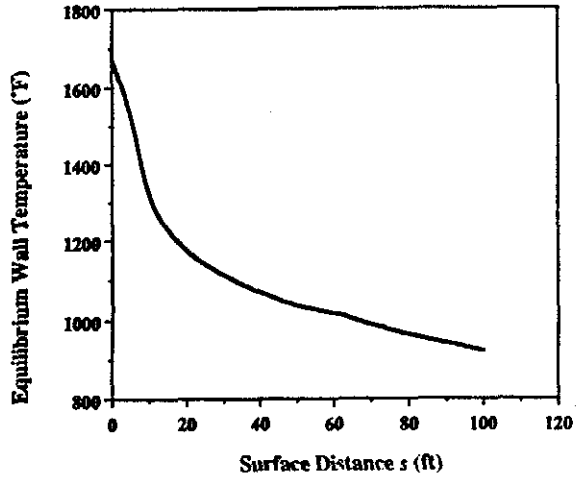

Figure 31. Wall Temperatures Along Centerline

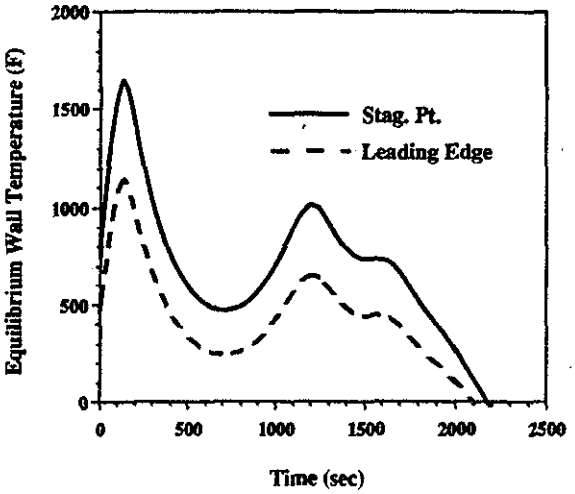

Figure 29. Wall Temperatures Along "Worst Case" Trajectory (emissivity = 0.8)

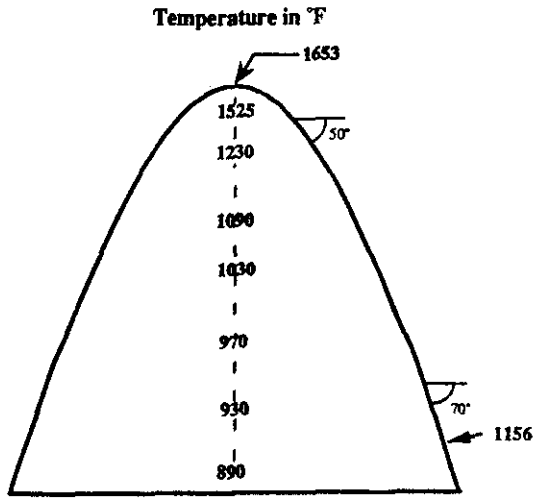

Figure 32. Temperature Distribution for the Medium L/D Forebody

Concluding Remarks

The Mars descent to surface vehicle will be designed to meet performance, scientific, and safety criteria. Selection of early Martian base locations will largely result from optimal iteration of these three concerns. This paper has discussed the role of vehicle performance in providing flexibility to meet a range of planned and off-nominal scientific and safety scenarios. Crossrange ability is a valuable performance parameter to be incorporated into the descent vehicle design. An alternative approach may be to use propulsive maneuvers during the transfer, capture, and descent phases in order to align the descent orbit periapsis with the desired landing site. Such use of propulsive "corrections" is assumed to be more costly in terms of propellant Initial Mass in Low Earth Orbit (IMLEO). Moreover, the resulting propellant needed to return the Mars' orbiting vehicle to the correct Earth return trajectory further increases IMLEO. These considerations led to the examination of optimizing vehicle crossrange.

A medium L/D descent aerobrake was chosen for study due mainly to the limitations of low L/D vehicles during the aerocapture portion and to the additional weight and complexity related to high L/D vehicles. Through descent trajectory optimization (via OTIS), this vehicle was shown to be capable of crossrange on the order of 1000 nmi. This is accomplished with heating rates and aeroshell temperatures well within current material capabilities. The safety aspects of daylight landings and assurance of reaching any previously established base show the medium L/D vehicle to be quite capable. The simulations presented in this paper were performed with end constraints for both velocity and altitude. The effects of varying these conditions in addition to those of angle of attack, descent orbit parameters, Mars atmospheric density, and landing delta V requirements must be studied to ultimately discover the range of optimal trajectories.

Acknowledgments

The work represented in this paper was performed under Boeing IR&D, 1990. Considerable thanks goes to Chris Weekly, an engineering student at the University of Alabama, for his help in compiling and documenting much of the data for this analysis. Thanks is also given to Dr Irwin Vas, Dr Niranjan Rao, and Mike Fouche for reviewing the results.

References

1. Woodcock, G.W. and Sherwood, S., "Engineering Aerobrakes For Exploration Missions", Boeing Aerospace and Electronics, Huntsville Division, 1989.

2. Hargraves, C.R. and Paris, S.W., "Direct Trajectory Optimization Using Nonlinear Programming and Collocation," Boeing Aerospace Company, 1987.

3. Tauber, M.E., Bowles, J.V., and Yang, L., "Atmospheric Environment During Maneuvering Descent from Martian Orbit," NASA, 1989.

4. NASA Contract NAS8-37857, "Space Transfer Concepts and Analysis for Exploration Missions", Second Quarterly Review, 1990.

5. Personal conversations with Gordon W. Woodcock, Boeing Aerospace and Electronics, Huntsville Division, 499 Boeing Blvd., MS JX-23, P.O. Box 240002, Huntsville, AL 35824-6402.

6. Braun, R.D., Powell, R.W., "Aerodynamic Requirements of a Manned Mars Aerobraking Transfer Vehicle", AIAA AFM Conference, August 1990.

7. Anderson, J.D., *Hypersonic and High Temperature Gas Dynamics*, McGraw-Hill Book Company, New York, 1989.

8. Hankey, W. L., "Re-Entry Aerodynamics", AIAA Education Series, 1988.

9. Justus C., "A Mars Global Reference Atmosphere Model (Mars-GRAM) for Mission Planning and Analysis.", AIAA-90-0004, 1990, School of Earth and Atmospheric Sciences, Georgia Institute of Technology, Atlanta, GA.

10. Vinh, N.X., Busemann, A., and Culp, R.D., *Hypersonic and Planetary Entry Flight Mechanics*, The University of Michigan Press, Ann Arbor, 1980.

11. Tauber, M.E., Bowles, J.V., and Yang, L., "The Use of Atmospheric Braking During Mars Missions", NASA, 1989.

12. Marvin, J. G. and Deiwert, G. S., "Convective Heat Transfer in Planetary Gases", NASA TR R-224, July 1965.

13. Lee, J. S. and Bobbitt, P. J., "Transport Properties at High Temperatures of CO_2-N_2-O_2-Ar", NASA Technical Note D-5476, Nov 1969.

14. Park, C., Davies, C. B., "Aerothermodynamics of Sprint-Type Manned Mars Mission", AIAA-89-0313, 1989.

15. Hartung, L. C., Sutton, K., and Brauns, F., "Equilibrium Radiative Heating Tables for Aerobraking in the Martian Atmosphere", NASA Technical Memorandum 102659, May 1990.